JOURNAL OF GEOPHYSICAL RESEARCH, VOL. 92, NO. C4, PAGES 3729–3740, APRIL 15, 1987

Hindcasts of Equatorial Sea Surface Dynamic Height in the Atlantic in 1982–1984

YVES DU PENHOAT AND YVES GOURIOU

Office de la Recherche Scientifique et Technique d'Outre-Mer, Brest, France

Two different wind data sets of the years 1982–1984 are used to force a linear multimode model of the tropical Atlantic ocean. We describe the variations of the equtorial slope in both cases and investigate the differences between the two runs. The main discrepancy occurs in 1983 for the amplitude of the seasonal signal all along the equator. Model results are also compared with observations (hydrocasts and inverted echo sounders) taken during the Programme Français Océan et Climat dans l'Atlantique Equatorial/Seasonal Response of the Equatorial Atlantic (FOCAL/SEQUAL) field experiment (July 1982 through October 1984). The contrast between 1983 and 1984 is well captured by the two runs, especially the abnormal flat topography of the sea surface along the equator in the first 3 months of 1984 due to an unusual basin wide relaxation of the equatorial wind stress. The major discrepancy between model results and observations is found during the upwelling periods east of 10°W, but at that time dynamic height measurements are too sparse to give a good description of these events.

1. INTRODUCTION

The surface topography of the equatorial Atlantic is subject to strong seasonal variations as revealed by the climatological studies [e.g., *Merle*, 1978]. The mean surface at the equator slopes downward to the east; it is rather flat in boreal spring and is the steepest in late boreal summer [*Merle and Arnault*, 1985]. The seasonal changes are linked with variations of surface winds which are primarily associated with the meridional migrations of the intertropical convergence zone (ITCZ) where northeasterly and southeasterly winds converge.

The Programme Français Océan et Climat dans l'Atlantique Equatorial/Seasonal Response of the Equatorial Atlantic (FOCAL/SEQUAL) experiment (July 1982 through October 1984) provides for the first time a quasi-synoptic data set which covered the entire tropical Atlantic Ocean for two seasonal cycles. A number of contributions (*Weisberg and Tang* [1987], *Katz* [1987], *Katz et al.* [1986], and *Weisberg and Colin* [1986], among others, have discussed the different types of data collected in 1983–1984 to demonstrate the differences between those 2 years. Most of their dynamical interpretations focus on how the springtime intensification of the trade winds at the equator takes place. This intensification is rather abrupt, occurring around mid-April in 1983 and 1 month later in 1984. There has been less discussion of the period when the wind field relaxes (November–December 1983), maybe because oceanographic sampling was less dense than it was during the rest of the experimental time [*Reverdin and du Penhoat*, 1987]. Moreover, wind sensors failed at Saint Peter and Saint Paul rocks from mid-November 1983 to mid-January 1984. It is after this transition period that an anomalously flat equatorial slope was observed with a very warm deep mixed layer and a rapid rise of dynamic topography in the eastern part of the basin [*Weisberg and Tang*, 1987; *Hisard and Hénin*, 1987]. Consequently, a large amount of heat has been redistributed from west to east [*Weisberg and Colin*, 1986].

Until recently, only climatological monthly averaged fields of surface wind stress were available, and numerous modeling studies have used these climatological winds to investigate the annual variability of the tropical Atlantic. These include (among others) a linear reduced gravity model [*Busalacchi and Picaut*, 1983], a multimode linear model [*du Penhoat and Treguier*, 1985] and a more sophisticated multilevel primitive equation model [*Philander and Pacanowski*, 1986]. Recently two sets of wind stresses have been made available for 1982–1984. The first one is a monthly averaged wind stress from ship reports [*Servain et al.*, 1985], whereas the second one is a daily wind stress field derived from the forecasting model of the European Center for Medium Range Weather Forecasting (ECMWF), Reading, England (V. Cardone, private communication, 1986).

This note is a first attempt to compare model results with observations for these two specific years. The model (section 2) is a simple linear multimode model which has been successful in describing the response of the tropical Atlantic to climatological winds. The two wind fields used to force the numerical model are presented in section 3. We describe in section 4 the model evolution of the surface dynamic height at the equator. Such an integrated quantity is expected to be well predicted as indicated by nonlinear models (at least for its large scales [*Cane*, 1979; *Philander and Pacanowski*, 1987]). We investigate the differences in model results forced with the two different forcings and compare these results with the surface dynamic height topography estimated from hydrographic legs [*Hisard and Hénin*, 1984, 1987] and, in some places, from inverted echo sounders (IES) and tide gauges [*Katz et al.*, 1986; *Katz*, 1987]. In section 5, conclusions will emphasize the differences contained in both wind patterns which are likely to play an important role in the adjustment of the equatorial slope as seen by this simple model.

2. THE MODEL

The model is a linear wind forced model of a stratified ocean and has been described in detail by *du Penhoat and Treguier* [1985] (hereinafter refered to as PT]. The equations are linearized about a background density profile $\bar{\rho}_\theta(z)$. Then, variables describing the circulation may be written as a sum of vertical standing modes; for the horizontal velocity components the pressure and density, we get

$$(u, v, p) = \sum_n (u_n, v_n, p_n)(x, y, t)A_n(z) \tag{1}$$

$$\rho_\theta = \bar{\rho}_\theta(z) - \frac{1}{g}\sum_n p_n(x, y, t)\frac{dA_n}{dz}$$

Paper number 7C0108.
0148-0227/87/007C-0108$05.00

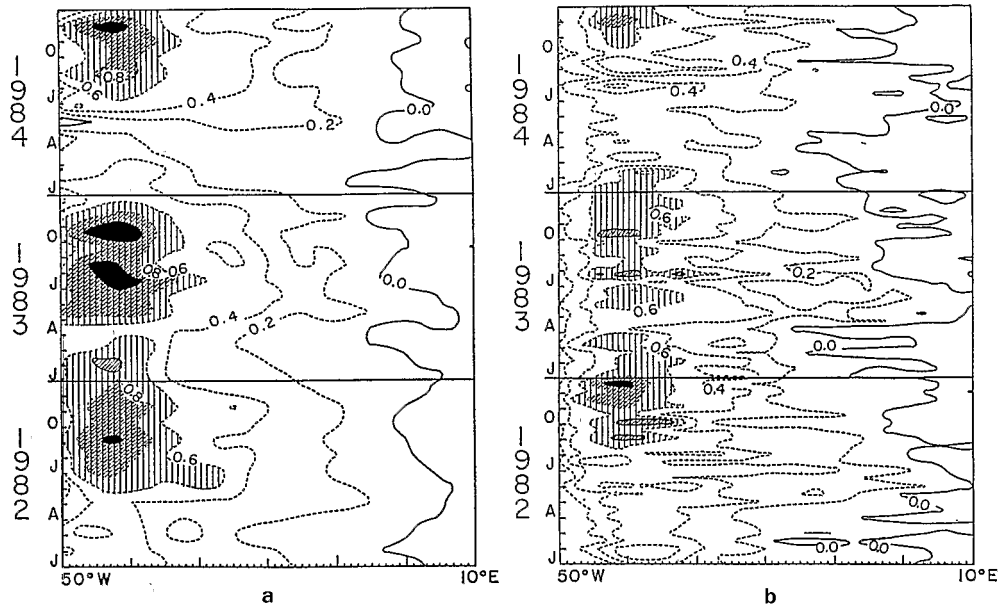

Fig. 1. Time-longitude plots of the zonal equatorial wind stress (in dynes per square centimeter): (*a*) monthly wind stress from SPB forcing and (*b*) 5-day-averaged wind stress from FSIIB forcing.

The vertical structure functions $A_n(z)$ are orthonormal vertical modes and are the solutions to an eigenvalue-eigenfunction problem that depends on stratification through the horizontally averaged buoyancy frequency $N(z)$ and top and bottom boundary conditions.

To find the horizontal structure, we must solve the shallow water equations for each baroclinic mode n using the long-wave low-frequency approximation [*Cane and Sarachik*, 1977, 1981].

$$\frac{\partial u_n}{\partial t} - \beta y v_n + \frac{\partial p_n}{\partial x} = F_n - r_n u_n \tag{2a}$$

$$\beta y u_n + \frac{\partial p_n}{\partial y} = G_n - r_n v_n \tag{2b}$$

$$\frac{1}{{c_n}^2}\frac{\partial p_n}{\partial t} + \frac{\partial u_n}{\partial x} + \frac{\partial v_n}{\partial y} = \frac{-r_n}{{c_n}^2} p_n \tag{2c}$$

Where r_n are damping coefficients and F_n and G_n are projections of the wind forcing on the vertical modes.

This set of equations is solved using an efficient numerical procedure [*Cane and Patton*, 1984]. It separates the eastward (Kelvin mode) and westward (long Rossby modes) energy propagation. A numerical scheme which is second-order in time and space, is used to calculate the long Rossby wave part of the flow. It is implicit and unconditionally stable, so the time step is limited by accuracy rather than a stability requirement [*Cane and Patton*, 1984]. The Kelvin wave component is solved exactly by integrating along characteristics. The boundary currents along the American continent coasts are not computed explicitly, as eastward propagating short Rossby waves generated at the western coast are no longer solved by (2). However, their influence on the interior flow is accounted for, using a proper boundary condition at the west coast [*du Penhoat et al.*, 1983].

The model basin is bounded by 50°W, 10°E, 18°N, 12°S. The Brazilian and Gulf of Guinea coasts are formed by removing a 8.5° latitude by 15° longitude rectangle in the southeast corner and a 12.5° latitude by 25° longitude rectangle in the northeast corner of the basin. For the interior flow close to the equator, a more realistic basin geometry is unlikely to have much effect [*du Penhoat et al.*, 1983]. The model grid is 0°5 latitude by 1° longitude. Further discussion of the model validity can be found in the work of PT and *Reverdin and du Penhoat* [1986] (see Reverdin and du Penhoat's Figure 1 for a sketch of the model geometry).

We will investigate primarily variations of dynamic topography along the equator. The sea surface dynamic height referred to 500 m is computed using the in situ density relation given by *Millero and Poisson* [1981], as was done by PT.

In this work, only the first three baroclinic modes are taken into account in computing the dynamic height. PT have shown that the first three modes account for 95% of the seasonal signal, as higher modes are more heavily damped and as the gravest modes dominate the solution at the surface. We choose a background density profile relevant for the FOCAL/SEQUAL period. It has been calculated using FOCAL profiles at the equator. The corresponding internal wave speed for the first three modes are respectively $C_1 = 2.19$ m/s, $C_2 = 1.29$ m/s and $C_3 = 0.89$ m/s. The second baroclinic mode is predominantly forced, as the wind forcing projection for the second mode is 2.4 times larger than that for the first mode and 3 times larger than that for the third mode.

3. THE WINDS

The wind field in the tropical Atlantic exhibits a strong seasonal signal [e.g., *Hellerman and Rosenstein*, 1983]. The principal feature is the presence of the intertropical convergence zone, which separates the prevailing northeasterly and southeasterly winds over most of the basin. In the easternmost part of the Gulf of Guinea, southerly to southwesterly winds prevail. Winds along the equator are weak when the ITCZ reaches its southernmost position close to the equator in boreal winter, and they get stronger as the ITCZ migrates northward in summer. However, year-to-year variations of its position are important, as was revealed by *Picaut et al.*

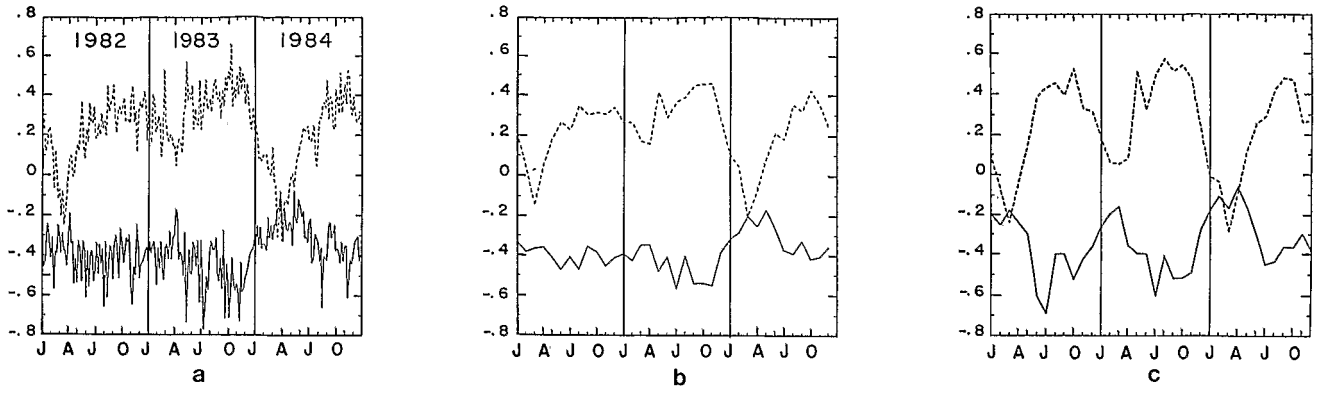

Fig. 2. Time series of wind stress around Saint Peter and Saint Paul rocks (in dynes per square centimeter): (*a*) 5-day-averaged wind stress from FSIIB, (*b*) monthly averaged wind stress from FSIIB, and (*c*) monthly averaged wind stress from SPB. Solid lines show τ^x; dashed lines show τ^y.

[1985]. The ITCZ remained in a position north of its normal position in spring 1983, whereas in early 1984 it stayed at a position unusually far south, straddling the equator and even extending south of the equator in the vicinity of the warmest sea surface temperature [*Horel et al.*, 1986]. It was also during this period that a double convergence line had its best definition. Consequently, winds were stronger than normal at the equator in early 1983 and were particularly weak for the same months in 1984. The intensification of the winds due to the northward migration of the ITCZ took place 1 month later in 1984 than in 1983 (mid-April in 1983, mid-May in 1984), as is revealed by wind measurements at Saint Peter and Saint Paul rocks.

Only a few in situ time series of wind measurements are available during the experiment, and they only partially indicate the large-scale wind forcing [*Colin and Garzoli*, 1987]. Two different gridded wind estimates have been constructed to provide a forcing function over the whole tropical Atlantic. The two wind fields which will force the model are as follows:

1. In the first experiment, the model was forced with monthly wind stress data set (hereinafter referred to as SPB) which was first constructed for the period 1964–1979 [*Servain et al.*, 1985], then updated through 1984 in order to cover the FOCAL/SEQUAL field experiment. Wind stress maps on a $2° \times 2°$ grid are constructed from ships reports averaged on $5° \times 2°$ boxes using objective analysis. Details of the method are given by *Picaut et al.* [1985]. The final product is presented as a pseudo wind stress, and the user has to choose the value of the drag coefficient C_d he believes to be the most appropriate. In this study, we choose $C_d = 1.2 \times 10^{-3}$ to be consistent with the formulation proposed by *Large and Pond* [1981]. In this experiment the time step has been chosen as 0.25 months. The spin-up is made by repeating the 1982 year for 10 years. In an earlier experiment the model was first spun up for 10 years with an average monthly mean wind stress obtained from the 21 years. (A discussion of the longer time series can be found in the work of *Reverdin and du Penhoat* [1987].) It turned out that slight differences between the two experiments occur only for the first 3 months of 1982, showing that the spin-up procedure will not affect model results for the FOCAL/SEQUAL period.

2. In the second experiment, the model has been forced with winds derived from the ECMWF forecast model. The wind stress is available on a $1.875° \times 1.875°$ grid and has been computed with a formula discussed by *Large and Pond* [1981]. Comparisons with data measurements and ship reports revealed systematic errors in ECMWF wind directions. These flaws were corrected assuming that SPB monthly mean wind direction is correct (V. Cardone, personal communication, 1986). We then use a final product called FOCAL/SEQUAL level 2B (hereinafter referred to as FSIIB), which is no longer close to the ECMWF product. For our purpose, the daily wind data have been averaged over 5 days. A 5-day time step is used in the numerical model, and the spin-up is made by repeating the 1982 year for 10 years.

In addition to the presence of higher-frequency variability in FSIIB, the wind data files exhibit some important differences at the equator. Particularly west of 25°W, SPB is more energetic and shows a stronger seasonal signal than FSIIB (Figure 1). This is also obvious in Figure 2, which shows the temporal variations of the wind stress components on a box centered around Saint Peter and Saint Paul rocks (0°55′N,

TABLE 1. Year Day of the Hydrographic Profiles Along the Equator During the Different FOCAL Cruises

FOCAL Cruise	35°W	28°–29°W	23°W	10°W	4°W	1°E	6°E
1	Oct. 30, 1982	Nov. 5, 1982	Oct. 19, 1982 Nov. 10, 1982	Nov. 15, 1982	Nov. 19, 1982	Nov. 14, 1982	Nov. 6, 1982
2	Jan. 27, 1983		Jan. 17, 1983	Feb. 5, 1983	Feb. 16, 1983	Feb. 14, 1983	Feb. 6, 1983
3	April 12, 1983	April 17, 1983	April 1, 1983	April 23, 1983	April 27, 1983	May 9, 1983	May 1, 1983
4	July 20, 1983	July 25, 1983	July 9, 1983	July 30, 1983	Aug. 4, 1983	Aug. 9, 1983	Aug. 2, 1983
5		Oct. 29, 1983	Oct. 15, 1983	Dec. 1, 1983	Nov. 23, 1983	Nov. 10, 1983	Nov. 17, 1983
6	Jan. 27, 1984	Jan. 21, 1984	Jan. 17, 1982	Feb. 9, 1984	Feb. 13, 1984	Feb. 22, 1984	Feb. 14, 1984
7	April 15, 1984	April 12, 1984	April 8, 1984	April 29, 1984	May 1, 1984 May 9, 1984	May 17, 1984	May 9, 1984 May 10, 1984
8	Aug. 5, 1984	Aug. 1, 1984	July 10, 1984 July 29, 1984	July 26, 1984	July 19, 1984	Aug. 8, 1984	July 31, 1984

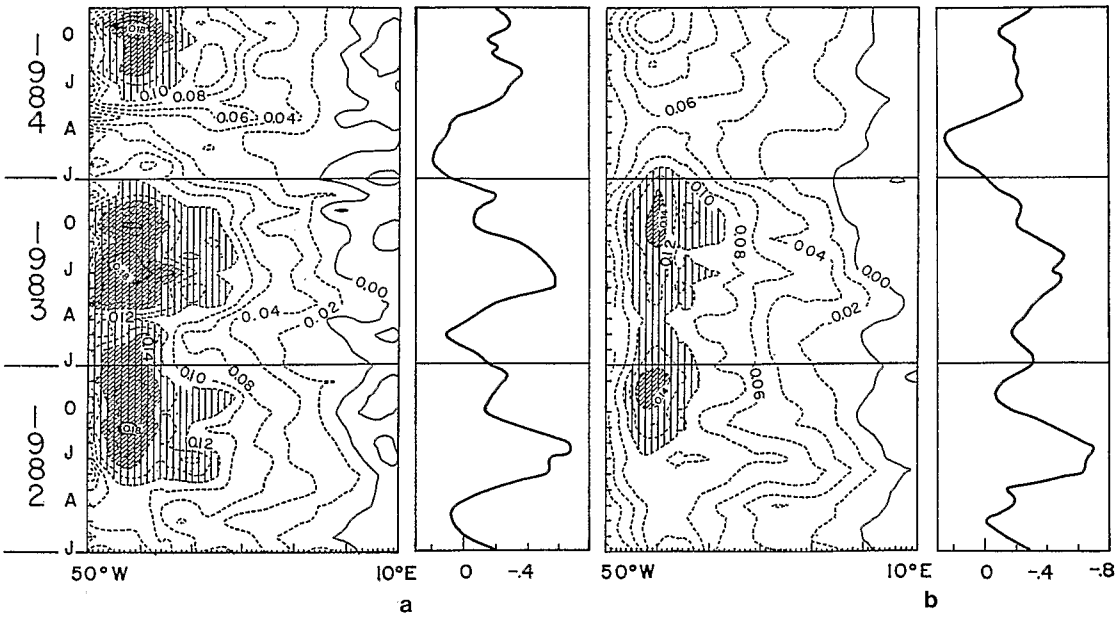

Fig. 3. Second Kelvin mode forcing ($b_2(x, t)$) for (*a*) SPB and (*b*) FSIIB. The curves in the panels to the right of the contour plots are Kelvin wave amplitude ($a_2(x_e, t)$) at the eastern coast.

29°20'W). In Figure 2*b*, FSIIB wind stress has been monthly averaged to make the two winds comparable. The most striking feature is the weakness of the seasonal cycle in 1983 in FSIIB, whereas it is still well marked in SPB. Another important difference, which will give evident contrast on model results, is the second intensification of the zonal wind stress present in SPB west of 35°W at the end of 1983, just before a strong relaxation in mid-December. Apart from these differences in the seasonal cycle, the two wind data files show similar characteristics from one year to the other, in particular the strong basinwide collapse of the trade winds at the equator in the early months of 1984.

It is interesting to note that the main differences among the 3 years take place during the first half of each year to the west of 30°W (Figure 1). In 1983 the relaxation of the zonal component of the wind stress is weak, whereas in 1984 it is well marked; the first half of 1982 seems close to the mean annual cycle.

4. Results

Sea surface dynamic height calculations from hydrographic legs are available all along the equator (Table 1; see also *Hisard and Henin* [1984]), but with the drawback that they are neither synoptic nor continuous. Travel times from the inverted echo sounders give useful information as a continuous record [*Katz*, 1987]. In contrast to the tropical Pacific Ocean, there are only very short reliable time series of sea level measurements and only two equatorial locations of sea level records during the FOCAL/SEQUAL field experiment (29°W and 7°E [*Katz et al.*, 1986]).

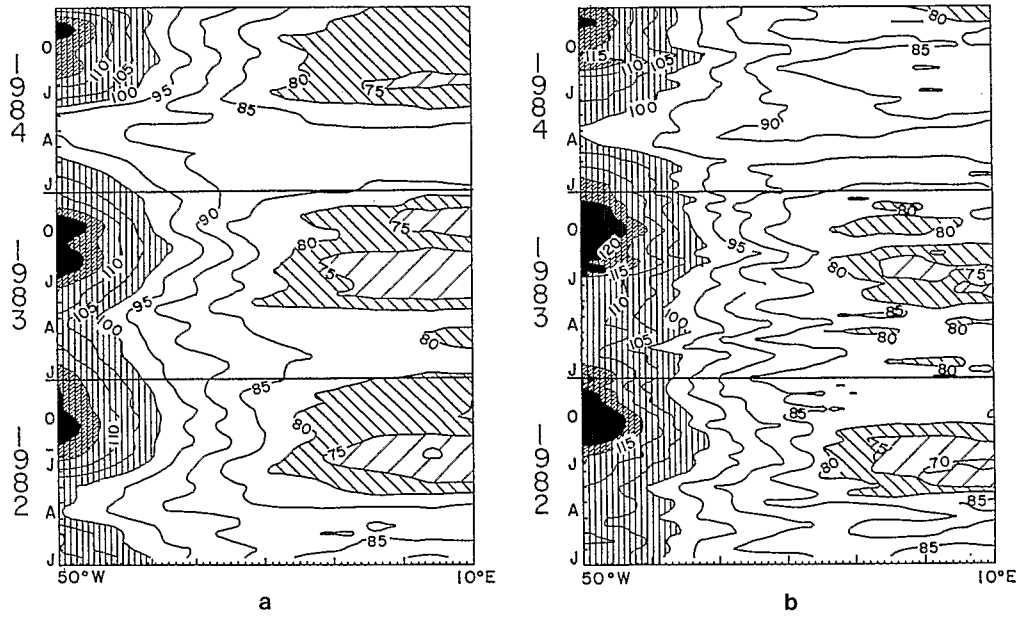

Fig. 4. Time longitude plot of the surface dynamic height along the equator for (*a*) the SPB run and (*b*) the FSIIB run.

As was pointed out by *Cane* [1984], the dynamics of the wind driven response on the equator is simple. The response of eastern equatorial and eastern coast regions are primarly determined by Kelvin waves impinging on the eastern boundaries, and the amplitude of the response is governed by the integral of zonal wind stress over the forced region. Kelvin waves and long Rossby waves, and their multiple reflections, give an interference pattern in which it is hopeless to focus on propagation of individual waves, at least at these low frequencies. The structure of the interference pattern will be dependent on time and spatial evolutions of the wind stress near the equator and on characteristics (internal speed) of the baroclinic modes determined from the background density.

Most of the height changes in the east are due to the zonal winds near the equator. This influence is measured by the evolution in space and time of the projection of the zonal forcing F on the Kelvin mode [*Cane*, 1984]:

$$b_n = \frac{2^{-1/2}}{D_n} \int_{ys}^{yN} \psi_0(y/L_n) F(x, y, t)\, dy/L_n$$

where

$$\psi_0(y) = (2\pi^{1/2})^{-1/2} e^{-y^2/2}$$

D_n is a coupling coefficient for the n mode (see PT), and L_n is the n mode equatorial radius of deformation.

In Figure 3 the contours of $b_2(x, t)$, projection of the forcing on the second baroclinic mode, are plotted for each run. The curves to the right of the contours are the amplitude of the second Kelvin mode $a_2(x_e, t)$ at the east coast. Most of the change in zonal wind stress occurs west of 20°W. The amplitude variations of $a_2(x_e, t)$ in the two runs differ especially in 1983: the decrease in the amplitude starts in August for the FSIIB run and continues monotonically until mid-March 1984 (interrupted only by a small secondary maximum in November). On the other hand, in SPB there is a secondary maximum in November followed by a steeper decrease with a minimum in February. This is due to an increase in the zonal wind stress in the west in October and an increase further east 1 month later. Figure 3 also shows the differences outlined in the preceding section: the lack of a well-defined seasonal signal in 1983 around 25°W in the FSIIB run and the presence of more pronounced gradient in the SPB run.

Equatorial Slopes

Figure 4 compares the temporal evolution of dynamic height topography along the equator for the two runs. The seasonal signal for the 3 years is more accentuated for the SPB run than for FSIIB. This is particularly true in the middle of the basin (15°W to 35°W). This reflects the differences in the wind files as pointed out in section 3 (see also Figure 1 and Figure 2). The strong relaxation of the wind stress (Figure 1) at the beginning of 1984 leads to a basinwide collapse of the dynamic equatorial slope in March–April. The resulting dynamic topography is unusually flat compared with the topography in early 1982 and 1983 in both runs. From November 1983 to April 1984 (Figure 5), the dynamic height drops at 50°W by about 24 dyn cm in the SPB run and by about 21 dyn cm in the FSIIB run, while it increases at 10°E by 5 dyn cm and 16 dyn cm, respectively. We can note a slightly reversed slope between 40°W and the eastern coast on FSIIB in April 1984. The time of the maximum relaxation of the equatorial slope in model runs is in April 1984, which agrees with observations: it corresponds to the time of the minimum of

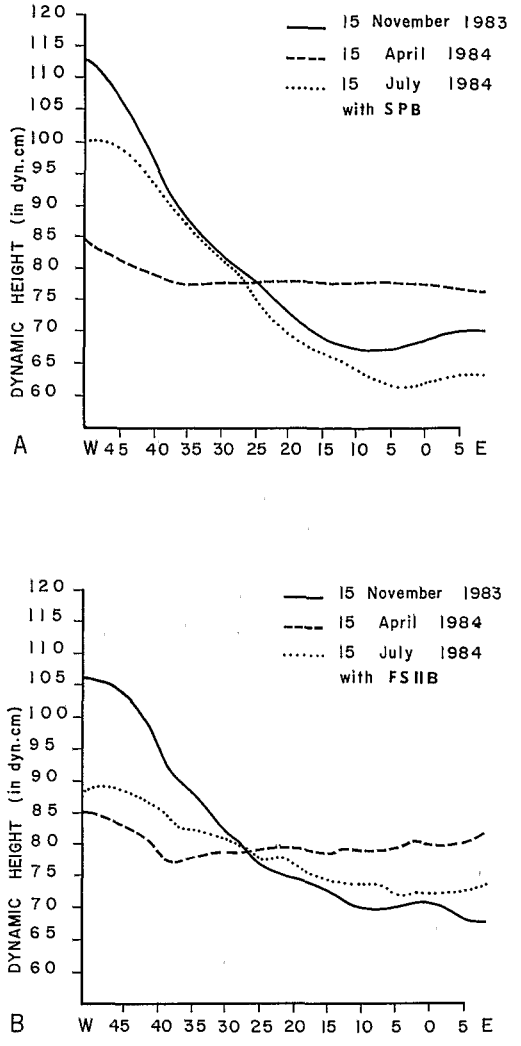

Fig. 5. Cross-equatorial slope for individual month for (*a*) the SPB run and (*b*) the FSIIB run.

the zonal pressure gradient along the equator calculated either between 34°W and 10°W from four IES (Figure 3 of *Katz* [1987]) or between 28°W and 4°W from temperature observations of equatorial moorings (Figure 3 of *Weisberg and Weingartner* [1986]).

It is more difficult to compare the slopes depicted by the FOCAL cruises and Figure 4 because cruise hydrocasts are not synoptic. Table 1 indicates the time of the different measurements. In Figure 6 we have reported the dynamic height along the equator for the FOCAL oceanic surveys (open diamonds) as given by *Hisard and Hénin* [1984, 1987]. Model values for both runs, sampled at the same position and same time, are also reported in Figure 6 (crosses). Solid lines superposed on the individual points are a third-order polynomial fit to the data. The model slopes generally agree with slopes as seen from the data.

We computed rms differences between the curves fit to FOCAL observations and the model fit for the two runs (Table 2). The rms differences vary between 1.41 dyn cm (FOCAL 2) and 5.9 dyn cm (FOCAL 4) for the SPB run and between 2.0 dyn cm (FOCAL 1) and 4.94 dyn cm (FOCAL 6) for the FSIIB run. The smallest rms values are found with the FSIIB run (except for FOCAL 2 and 3). Larger differences occur for the two runs for FOCAL 5 and FOCAL 6 when the wind stress starts to relax across the basin. This suggests that

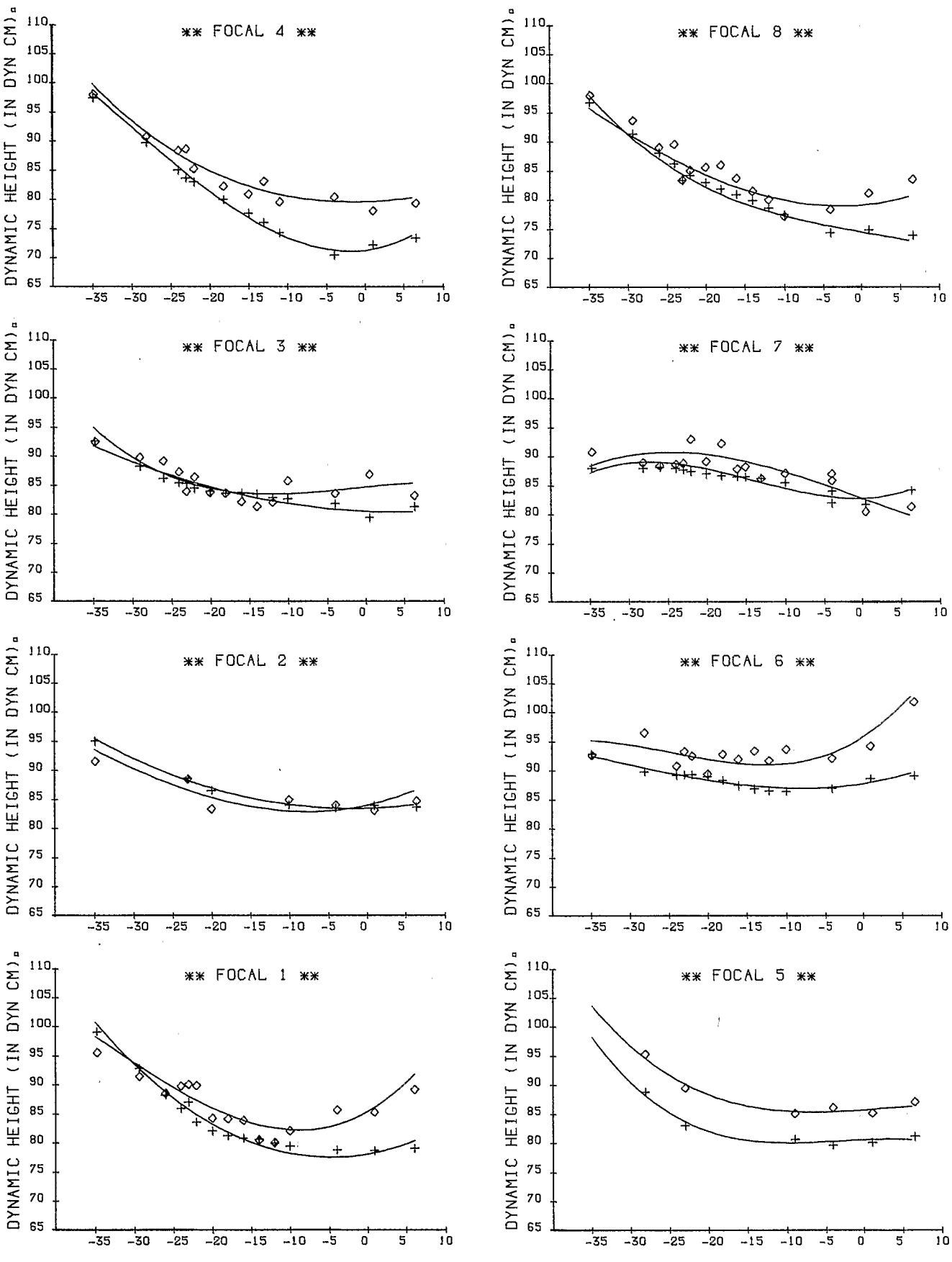

Fig. 6. Cross-equatorial slopes as seen by FOCAL cruises (open diamonds) and by the model (crosses) for (*a*) the SPB run and (*b*) the FSIIB run. Solid lines are a third-order polynomial adjustment.

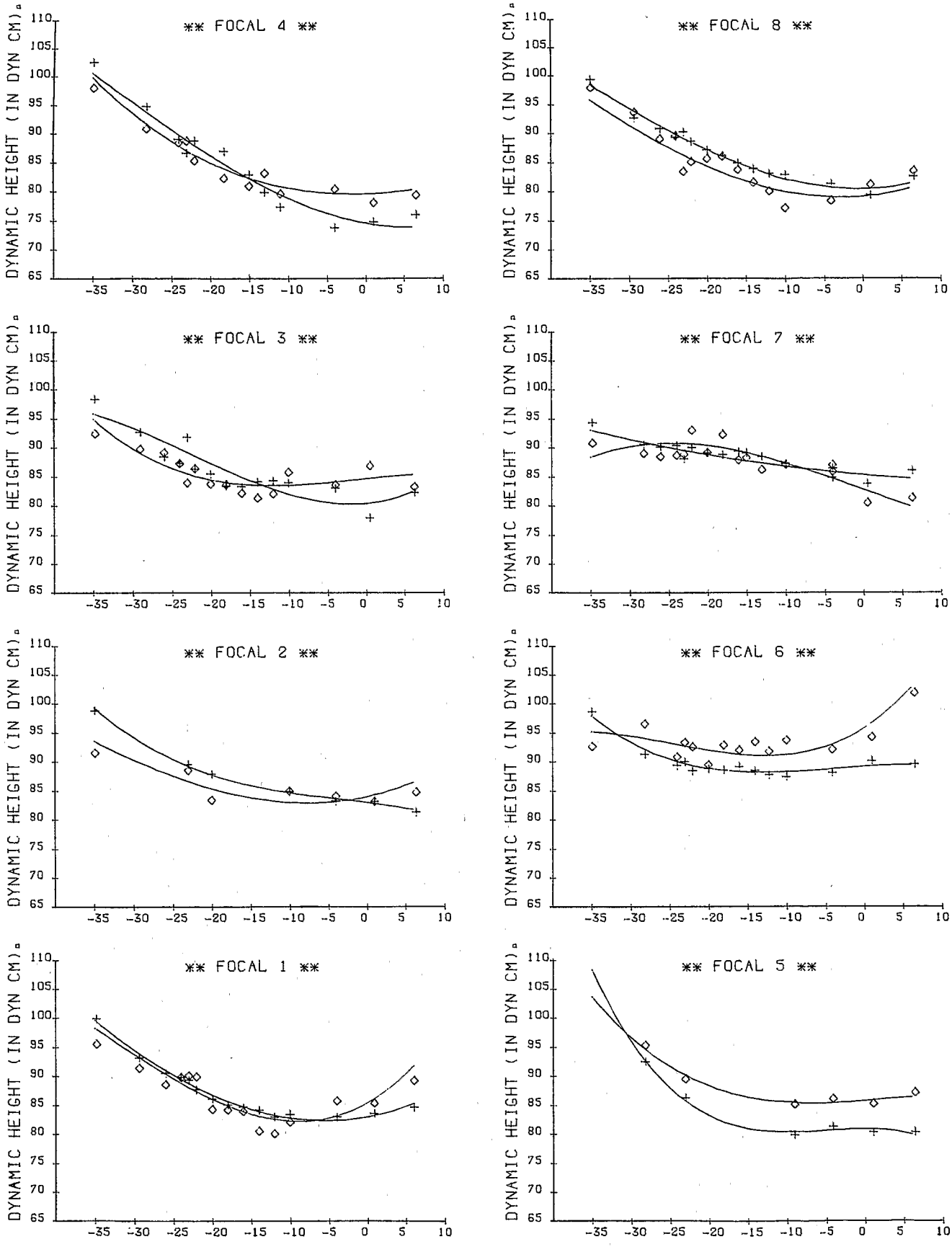

b

Fig. 6. (continued)

TABLE 2. Root-Mean-Square Differences (in Dynamic Centimeters) Between Curves Fit to FOCAL Observations (Data) and Model Fits for the Two Runs (FSIIB and SPB)

FOCAL Cruise	FSIIB − Data	SPB − Data	FSIIB − SPB
1	2.00	5.00	3.84
2	2.83	1.41	1.50
3	3.12	2.66	2.66
4	3.12	5.90	4.29
5	4.62	5.89	3.41
6	4.94	5.89	1.90
7	2.15	2.26	2.45
8	2.35	3.34	5.07

both wind stress files are questionable when the wind stress collapses at a basinwide scale at the end of 1983. (This also can be seen in model time series, e.g., Figure 8).

Owing to the nonsynopticity of FOCAL hydrocasts along the equator, it is difficult to have the real transequatorial slope of the sea surface, especially during periods of rapid temporal evolution: for example, we observe an eastward tilt in April 1984 (Figure 5), whereas the model runs sampled as FOCAL 7 observations show a westward tilt (Figure 6). It is more evident in the calculation with FSIIB winds. This is because the time lag exceeds 1 month between the measurements west of 20°W and the measurements east of 0° where the dynamic topography has started to drop because of the seasonal intensification of the wind stress.

The rms differences between the two runs are in the same range as differences between models and observations (Table 2): 1.90 to 5.07 dyn cm. The maxima are observed during the upwelling season (FOCAL 4 and FOCAL 8) which is not as well described by the SPB run as by the FSIIB run. The upwelling is more intense in the Gulf of Guinea in the SPB run, and the westward slope at the west is more pronounced in response to the stronger wind stresses there in the SPB forcing.

A more quantitative evaluation of the slope is given in Figure 7. We calculate the dynamic height difference between 29°W and 6°E from the FSIIB run and compare it with Figure 2 of *Katz et al.* [1986], which gives the same difference computed from tide gauge records. The model and tide gauge differences present similar variations. However, from the middle of 1983 to the beginning of 1984, there is a 2-month lag between the two curves: the minima are situated in early April with the model and in early February with the tide gauges. The difference in dynamic height between 28°W and 6°E includes both the region of slope up to the west in the central Atlantic and the eastward slope in the Gulf of Guinea. As was pointed out by *Katz et al.* [1986], this does not mean that the curve minima are a basinwide reversed tilt. The disagreement between model results and observations is due to the too moderate reversed slope in the east (or its absence) in the model output (it is also obvious in Figure 6) and could also be due to the difference between real wind and model winds for the relaxation at the end of 1983, as was pointed out earlier. The inclusion of nonlinear effects will probably enhance the reversal of the tilt [*Philander and Pacanowski*, 1987]. The time of the minimum seems to agree between hydrocasts and tide gauge data. However, we must again be careful in analyzing the hydrocast data differences, because of the nonsynopticity of measurements at 29°W and 6°E. For example, the FOCAL 7 difference is doubtful because the measurement at 29°W was made on April 12, 1984, while that at 6°E was made a month later, on May 10. In 1984, it is

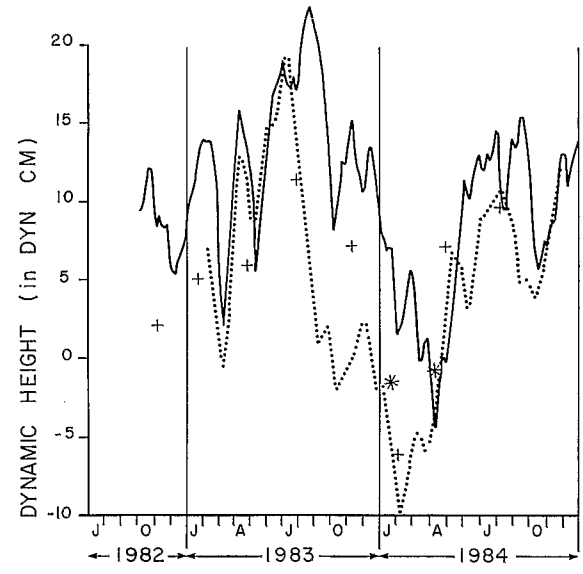

Fig. 7. Dynamic height differences between 29°W and 6°E as seen by FSIIB (solid line), by the tide gauges (dotted line) and FOCAL cruises (crosses). Asterisks are interpolated values (see text).

during this period that the intensification of the wind stress begins at the equator and the sea surface topography undergoes rapid changes. This can be seen in Figure 6: the dynamic height at 6°E drops 20.8 dyn cm between February 14 and May 10, 1984 (FOCAL 6 and FOCAL 7), compared with a drop of 9.6 dyn cm at 29°W between January 21 and April 12. Asterisks in Figure 7 represent the difference in dynamic height between 29°W and 6°E with the values at 6°E being linearly interpolated in time between FOCAL 6 and FOCAL 7 at the date of measurement at 29°W. This shows a substantial difference with points calculated as if measurements at 29°W and 6°E were synoptic. We are then unable to have a precise determination of the time of the pressure gradient minimum from FOCAL measurements. The comparison (not shown) of dynamic height difference between 34°W and 10°W and the IES as presented by *Katz et al.* [1986] agrees, with a maximum in late July 1983 and a minimum in early April 1984 in both calculations. The same conclusion holds for the calculation carried out by *Weisberg and Weingartner* [1986] for differences between 28°W and 4°W from moorings.

Time Series

Figure 8 shows time series of sea surface dynamic height along the equator sampled at fixed longitudes (35°W, 29°W, 10°W, 4°W, and 1°E) calculated from model output for the two runs. The values (averaged between 0°, 30°N and 0°, 30°S) computed from FOCAL hydrographic legs are also reported (shown by crosses) as well as IES time series (at 35°W, 29°W, and 10°W; dotted lines). Root-mean-square differences between model runs and data are also computed (Table 3), although hydrographic casts are not very numerous. However, they are well distributed in time.

At 35°W the dynamic height in the FSIIB run is always above hydrocast observations and IES. We got a better agreement with the SPB run with a rms difference half as large (rms = 2.45 dyn cm (Table 3)) as with the FSIIB run (rms = 4.92 dyn cm). For both runs (Figure 8), the agreement is good in amplitude and phase with, however, a 2-month shift of the minimum in 1983 in the SPB run. Hydrocast and IES data suggest that the minimum occurs in February–March 1983, more than a month prior to the seasonal intensification

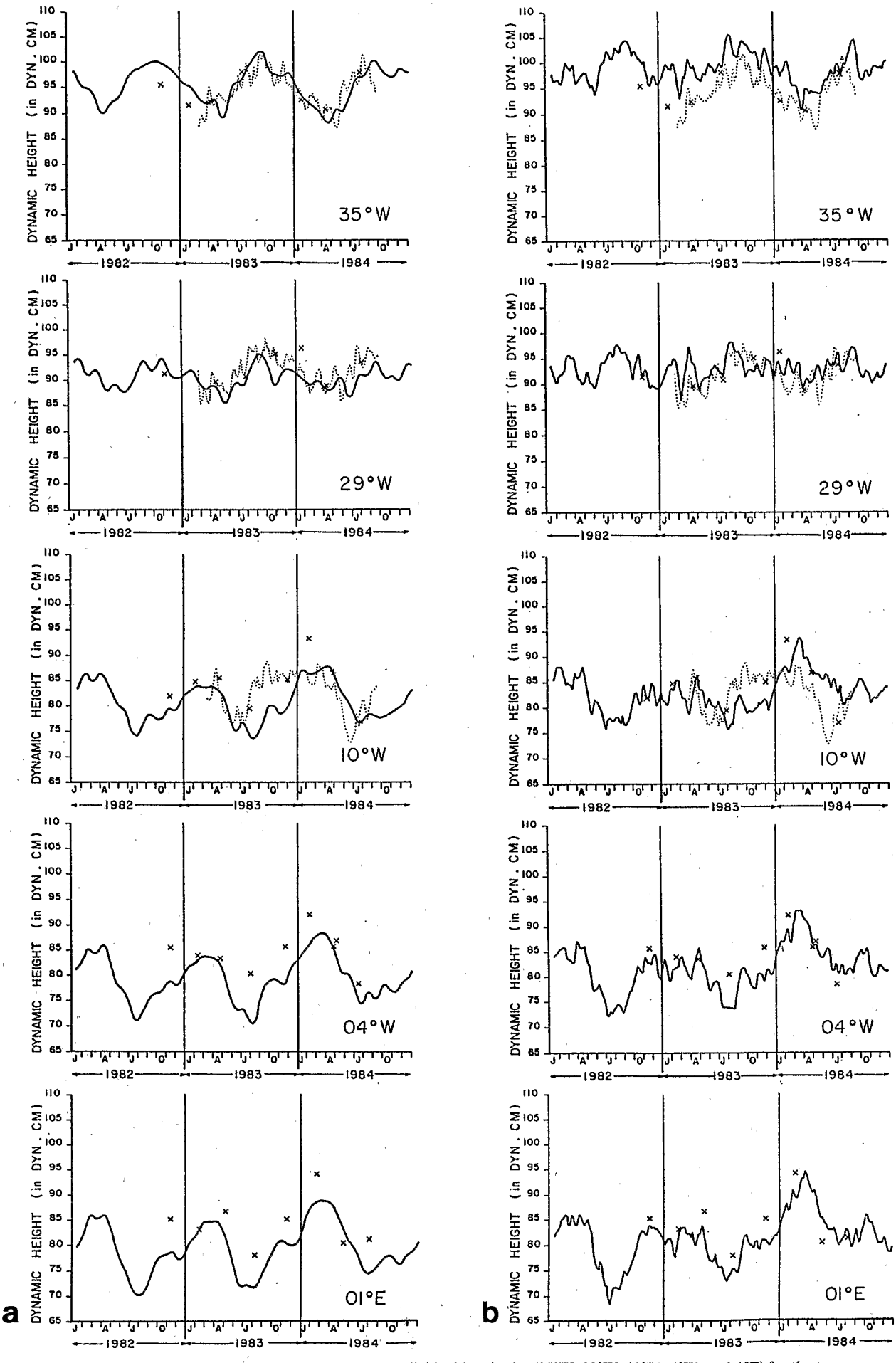

Fig. 8. Time series of dynamic height (solid line) at individual longitudes (35°W, 29°W, 10°W, 4°W, and 1°E) for the two runs (*a*) SPB and (*b*) FSIIB.

TABLE 3. Root-Mean-Square Differences (in Dynamic Centimeters) Between FOCAL Observations (Data) and Model Results Sampled as Observations at Different Longitudes

Longitude	FSIIB − Data	SPB − Data
35°W	4.92	2.45
28°W	2.35	3.59
10°W	3.41	3.95
4°W	3.76	5.27
1°E	3.64	5.33

of the zonal wind stress. In the SPB run, the seasonal signal of the dynamic height is well defined with the seasonal minima occurring in April in 1982 and 1984 and in early May in 1983. This suggests that the climatology used for objectively mapping the wind stress has an influence in regions where wind observations are not numerous.

At 29°W the seasonal signal exhibits a smaller amplitude than it exhibits elsewhere along the equator, in both runs and in observations. In FSIIB, intermediate frequency oscillations dominate the seasonal signal; the crest to crest amplitude of these oscillations is as large as the seasonal signal depicted by the IES (10 dyn cm). The main difference between the two runs takes place at the end of 1983 and the beginning of 1984: the FSIIB run exhibits a plateau from October 1983 to March 1984 which seems to be confirmed by hydrocast measurements (but not by IES). On the other hand, the model response to SPB is close for the 2 years and does not show such a feature. This can be explained by the difference in wind stress variations west of 29°W: the decrease of the wind stress is more important in SPB than in FSIIB (Figures 1 and 2) in early 1983.

Further east, differences between the two runs' experiments are more evident, especially in 1983. With FSIIB forcing, seasonal variations of dynamic height are weak, as the wind stress remains stronger than normal at the equator. It leads, for instance at 10°W and 4°W, to a plateau modulated by intermediate frequency variations from October 1982 to April 1983. This is confirmed by FOCAL cruise measurements and also by a mooring at 4°W [*Weisberg and Colin*, 1986; *Weisberg and Tang*, 1987]. This feature is not reproduced in the SPB run, where the dynamic height increases monotonically from July 1982 to February 1983. It is worth noting that during this period of time, at 10°W, both runs seem close to the observed dynamic height (rms differences equal 3.41 dyn cm for FSIIB and 3.95 dyn cm for SPB), although their temporal evolutions are different. At 4°W (and 1°E), there is also a plateau from October 1982 to April 1983 in FSIIB (as well as in observations) but not in SPB. The SPB run is not adjusted to the data as it is at 10°W (see rms differences in Table 3). This tends to show that the FSIIB run is more representative of this period in the eastern part of the basin.

As a consequence of the basinwide relaxation of the wind stress starting around November 1983, the dynamic height increases, reaching an unusually high surface height in early 1984 in both runs. This is more accentuated in FSIIB (maximum at the end of March). The IES record at 10°W does not indicate a high dynamic height as do hydrocasts, (Figure 8) and no reason has yet been given to explain the different results from the two observational methods [*Katz et al.*, 1986].

We can note a time shift between the observed dynamic height increase and the modeled one after the 1983 seasonal upwelling (FOCAL 5 and 6). In both model wind fields (Figure 1 and Figure 3), there is a second intensification of the zonal wind stress in October–November 1983 just before the relaxation, which prevents a more rapid increase of dynamic height. It would suggest that in 1983 the relaxation scenario of the model winds does not accurately represent the real wind.

The 2 years are less contrasted in SPB run than in FSIIB. Again, we believe that this is due to the weight given to climatology in the processing method for SPB winds.

A major difference between the model time series and observations is the relative intensities of the seasonal upwelling in 1983 and 1984. In both experiments, the 1983 upwelling is more pronounced than the 1984 one, as is shown by the minimum of dynamic height (Fig. 8 at 10°W, 4°W, and 1°E). This can be related to the wind forcing, which is more energetic in 1983 than 1984 (Figure 1 and Figure 4). On the other hand, IES at 10°W [*Katz*, 1987] and hydrographic cruises [*Hisard and Henin*, 1987] at 10°W and 4°W show a stronger upwelling in 1984. While the time evolution of the dynamic height from its minima in summer 1983 to its maxima in early 1984 agrees with hydrocast measurements east of 10°W (Figure 7), the amplitude of the decrease in 1984 is much smaller than is indicated by FOCAL 6, FOCAL 7, and FOCAL 8 measurements.

With the FSIIB forcing, short-lived events are present in the simulation, due to the presence of intermediate frequencies in the wind forcing. We ran the model again with the FSIIB wind stresses averaged over a month (time step = 0.25 month). Figure 9 shows time series obtained at individual points along the equator. All the major features discussed above are maintained, and of course, most of the high-frequency variations have been smoothed out.

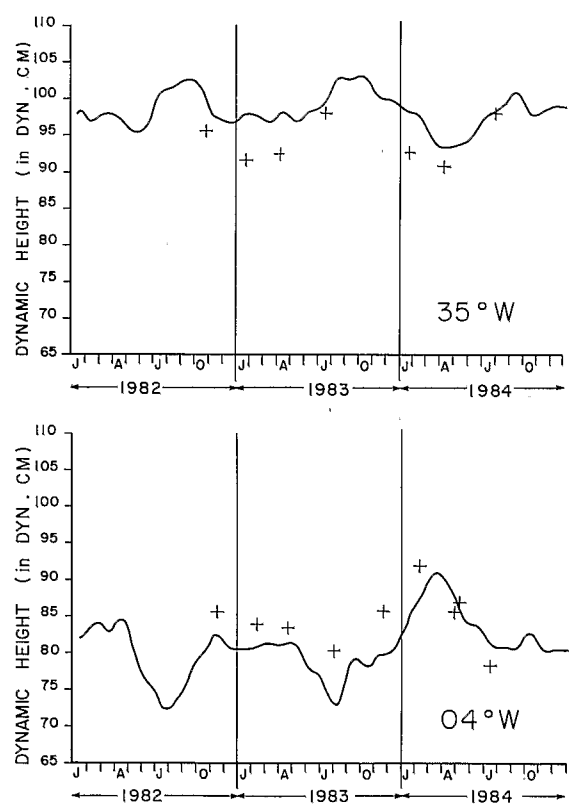

Fig. 9. Time series of model dynamic height at individual longitudes using monthly averaged FSIIB values. Observations of FOCAL cruises are shown by crosses.

5. CONCLUSION

In this note, we have forced a linear model with two different wind sets. The model pattern results from the interference of the directly forced long waves, eastward propagating Kelvin waves, and westward propagating Rossby waves and their subsequent reflections on ocean boundaries.

We have compared dynamic height along the equator computed by the model and calculated from direct measurements during the FOCAL/SEQUAL period. It is a first step to determine the quality of the hindcasts using simultaneous wind forcing and observations in the equatorial Atlantic for specific years. Although they are not very numerous, the data are sufficiently well distributed in space and time to provide information on the relative quality of the two runs.

There are uncertainties on the forcing functions. The two sets of wind stresses exhibit some important disparities. SPB wind has a well-defined seasonal signal, especially in the western part of the basin, which could be due to an excessive influence of the climatological guess field in area where ship wind observations are scarce. Therefore the model response to the SPB forcing shows a clear seasonal cycle which leads to a less important contrast between 1983 and 1984 in SPB than FSIIB. East of 10°W, for example, the SPB run does not reproduce the weak seasonal modulation of the dynamic height in the first half of 1983.

High frequencies are also present in the FSIIB file (and of course are not present in the SPB monthly averaged wind). These frequencies do not change the overall tendency, but they give rise to more rapid fluctuations in the oceanic response. These fluctuations are small compared with the seasonal signal except at 29°W, were they are almost as energetic.

Differences between model runs and observations are noted during the upwelling periods east of 10°W: the upwelling is more intense in 1983 than in 1984 in both model runs. It does not seem to be confirmed by the observations. However, the hydrocast measurements are too scarce to capture the upwelling period. It is not clear whether this difference is due to a flaw in the wind stress files or rather to other phenomena which are not taken into account in the model. Another difference between observations and model runs is the time shift observed in the second half of 1983 (FOCAL 5 and FOCAL 6): it is more visible at the east where the dynamic height increase earlier in observations. This suggests that the model forcing does not accurately represent the real winds for this period.

Aside from these disparities, the agreement between model results and observations is good (rms differences are generally smaller for FSIIB than for SPB). Both runs agree in depicting the strong contrast between the 2 years. They show an unusually flat equatorial slope in early 1984, when the equatorial wind stress collapsed at the basin scale with an abnormally high dynamic topography in the eastern part of the basin. As was shown by *Weisberg and Colin* [1986], at 4°W the vertical integrated temperature between 0 and 110 m peaks in February 1984 and starts to decrease at the end of March; the model time series agree (Figure 8).

This experiment demonstrates that it is possible to describe accurately the seasonal and interannual changes of integrated quantity such as dynamic height with a simple linear model. To improve the agreement with observations would require a better description of the surface wind field throughout the equatorial band. More model validations will be carried out in the near future as more observations for the FOCAL/SEQUAL period become available and as fully three-dimensional models are run forced with the FSIIB wind stress.

Acknowledgments. Hydrocast data were kindly provided by B. Piton, P. Hisard, and C. Henin, and IES data were provided by E. Katz. Thanks are due to M. Cane, G. Reverdin, and E. Katz for helpful comments and suggestions. This work is part of the FOCAL program, and financial support was from the Programme National d'Etude de la Dynamique du Climat.

REFERENCES

Busalacchi, A. J., and J. Picaut, Seasonal variability from a model of the tropical Atlantic Ocean, *J. Phys. Oceanogr., 13*, 1564–1588, 1983.

Cane, M. A., The response of an equatorial ocean to simple wind stress patterns, II, Numerical results, *J. Mar. Res., 37*, 253–299, 1979.

Cane, M. A., Modelling sea level during El Niño, *J. Phys. Oceanogr., 14*, 1864–1874, 1984.

Cane, M. A., and R. J. Patton, A numerical model for low frequency equatorial dynamics, *J. Phys. Oceanogr., 14*, 1853–1863, 1984.

Cane, M. A., and E. S. Sarachik, Forced baroclinic ocean motions, II, The linear equatorial bounded case, *J. Mar. Res., 35*, 395–432, 1977.

Cane, M. A., and E. S. Sarachik, The response of a linear baroclinic ocean to periodic forcing, *J. Mar. Res., 39*, 651–693, 1981.

Colin, C., and S. L. Garzoli, In situ wind measurements and ocean response in the equatorial Atlantic during the Programme Français Océan et Climat dans l'Atlantique Equatorial/Seasonal Response of the Equatorial Atlantic Experiment, *J. Geophys. Res.*, in press, 1987.

du Penhoat, Y., and A. M. Treguier, The seasonal linear response of the tropical Atlantic Ocean, *J. Phys. Oceanogr., 15*, 316–329, 1985.

du Penhoat, Y., M. A. Cane, and R. J. Patton, Reflections of low frequency waves on partial boundaries, in *Hydrodynamics of the Equatorial Oceans*, edited by J. C. Nihoul, pp. 237–258, Elsevier, New York, 1983.

Hellerman, S., and M. Rosenstein, Normal monthly wind stress over the world ocean with error estimates, *J. Phys. Oceanogr., 13*, 1093–1104, 1983.

Hisard, P., and C. Hénin, Zonal pressure gradient, velocity and transport in the Atlantic Equatorial Undercurrent from FOCAL cruises (July 1982–February 1984), *Geophys. Res. Lett., 11*, 761–764, 1984.

Hisard, P., and C. Hénin, Response of the equatorial Atlantic Ocean to the 1983–1984 wind from the Programme Français Océan et Climat dans l'Atlantique Equatorial cruise data set, *J. Geophys. Res.*, in press, 1987.

Horel, J. D., V. E. Kousky, and M. T. Kagano, Atmospheric conditions in the Atlantic sector during 1983 and 1984, *Nature, 322*, 248–251, 1986.

Katz, E. J., Seasonal response of the sea surface to the wind in the equatorial Atlantic, *J. Geophys. Res., 92*(C2), 1885–1893, 1987.

Katz, E. J., P. Hisard, and J. M. Verstraete, Annual change of the sea surface slope along the equator of the Atlantic Ocean in 1983 and 1984, *Nature, 322*, 245–247, 1986.

Large, W. G., and S. Pond, Open ocean momentum flux measurements in moderate to strong winds, *J. Phys. Oceanogr., 11*, 324–336, 1981.

Merle, J., Atlas hydrologique saisonnier de l'Océan Atlantique intertropical, *Trav. Doc. ORSTOM, 82*, 184 pp., 1978.

Merle, J., and S. Arnault, Seasonal variability of the surface dynamic topography in the tropical Atlantic Ocean, *J. Mar. Res., 43*, 267–288, 1985.

Millero, F. J., and A. Poisson, International one atmosphere equation of state of sea water, *Deep Sea Res., 28*, 625–629, 1981.

Philander, S. G. H., and R. Pacanowski, A model of the seasonal cycle of the tropical Atlantic Ocean, *J. Geophys. Res., 91*(C12), 14,192–14,206, 1986.

Philander, S. G. H., and R. Pacanowski, Non linear effects in the seasonal cycle of the tropical Atlantic Ocean, *Deep Sea Res., 34*, 123–137, 1987.

Picaut, J., J. Servain, P. Lecomte, M. Seva, S. Lukas, and G. Rougier, *Climatic Atlas of the Tropical Atlantic Ocean Wind Stress and Sea Surface Temperature 1964–1979*, 467 pp., Université de Bretagne Occidentale, Brest, France, 1985.

Reverdin, G., and Y. du Penhoat, Modeled surface dynamic height in 1964–1984: An effort to assess how well the low frequencies in the equatorial Atlantic were sampled in 1982–1984, *J. Geophys. Res.*, *92*(C2), 1899–1913, 1987.

Servain, J., J. Picaut, and A. Busalacchi, Interannual and seasonal variability of the tropical Atlantic Ocean depicted by sixteen years of sea surface temperature and wind stress, in *Coupled Ocean-Atmosphere Models, 16th Liège Colloquium on Ocean Hydrodynamics*, edited by J. C. Nihoul, pp. 211–237, Elsevier, New York, 1985.

Weisberg, R. H., and C. Colin, Equatorial Atlantic Ocean temperature and current variations during 1983 and 1984, *Nature*, *322*, 240–243, 1986.

Weisberg, R. H., and T. Y. Tang, Further studies on the response of the equatorial thermocline in the Atlantic Ocean to the seasonally varying trade winds, *J. Geophys. Res.*, in press, 1987.

Weisberg, R. H., and T. J. Weingartner, On the baroclinic response of the zonal pressure gradient in the equatorial Atlantic Ocean, *J. Geophys. Res.*, *91*(C10), 11,717–11,725, 1986.

Y. du Penhoat and Y. Gouriou, Antenne ORSTOM, Centre IFREMER, B. P. 337, 29273 Brest, France.

(Received August 29, 1986;
revised December 5, 1986;
accepted January 9, 1987.)